



Spin order and lattice frustration in optimally doped manganites: A high-temperature NMR study

N. Panopoulos, D. Koumoulis, G. Diamantopoulos, M. Belesi, M. Fardis, M. Pissas, and G. Papavassiliou
Institute of Materials Science, NCSR, Demokritos, 153 10 Aghia Paraskevi, Athens, Greece

(Received 8 September 2009; revised manuscript received 1 November 2010; published 1 December 2010)

Understanding the complex glassy phenomena, which accompany polaron formation in optimally doped manganites (ODMs) is a cumbersome issue with many unexplained perspectives. Here, on the basis of ^{139}La and ^{55}Mn nuclear magnetic resonance (NMR) measurements, performed in the temperature range 80–900 K we show that glass freezing, observed in the paramagnetic (PM) phase of ODM $\text{La}_{0.67}\text{Ca}_{0.33}\text{MnO}_3$, is not a random uncorrelated process but the signature of the formation of a genuine spin-glass state, which for $T < T_c$ consolidates with the ferromagnetic (FM) state into a single thermodynamic phase. Comparison with NMR measurements performed on $\text{La}_{1-x}\text{Ca}_x\text{MnO}_3$ systems for $0.0 \leq x \leq 0.41$ and ODM $\text{La}_{0.70}\text{Sr}_{0.30}\text{MnO}_3$, demonstrates the key role played by the local lattice distortions, which control (i) the stability of the spin-glass phase component and (ii) the kind (first or second order) of the PM-FM phase transition. The experimental results are in agreement with the predictions of the compressible random bond-random field Ising model, where consideration of a strain field induced by lattice distortions is shown to invoke at T_c a discontinuous first-orderlike change in both the FM and the “glassy” Edwards-Anderson order parameters.

DOI: [10.1103/PhysRevB.82.235102](https://doi.org/10.1103/PhysRevB.82.235102)

PACS number(s): 75.47.Lx, 75.50.Lk, 76.60.-k, 75.30.Et

I. INTRODUCTION

The study of strong electron correlations in transition-metal oxides unveiled a complex world of interweaving properties, concerning their spin, charge, and crystal structure. Predominant examples are high-temperature superconducting cuprates and hole-doped manganites. Competition among different interactions in these systems generates spectacular phenomena, such as the formation of charge and spin stripes,^{1–4} mesoscopic phase separation,^{5–7} and the colossal magnetoresistance (CMR) effect.^{8,9} At the same time frustration of interactions gives rise to the appearance of freezing and glassiness,^{10,11} expressed with slow relaxation, aging, and other signatures of glassy systems.^{12–14} However, it is not yet clear, whether this kind of glassiness is a fundamental property of strongly correlated electron systems, or the consequence of quenched disorder, which produces uncorrelated charge and spin fluctuations.

In the case of hole-doped manganites, exemplified by the prototype $\text{La}_{1-x}\text{Ca}_x\text{MnO}_3$ (LCMO) family, substitution of La^{3+} ions with the divalent alkaline-earth metal ion Ca^{2+} , invokes the replacement of Jahn-Teller (JT) active Mn^{3+} ions with JT inactive Mn^{4+} ions. Here, frustration is generated by competition between (i) coherent JT lattice distortions, which favor charge localization, and (ii) the double-exchange mechanism, which favors motion of e_g electrons between adjacent ferromagnetic (FM) ordered Mn^{3+} and Mn^{4+} ions, and tends to smooth out lattice distortions. In the low-doping regime, $0 \leq x \leq 0.2$, the crystal structure is orthorhombic with coherently JT distorted oxygen octahedra. This is known as the O' phase (Fig. 1). From the magnetic point of view, the ground state is antiferromagnetic insulating, becoming FM insulating for $0.1 \leq x$. By further increasing doping, the FM metallic phase is imposed in the doping range $0.2 < x < 0.5$, and the ground state becomes that of an isotropic FM metal. This major change in the electronic properties is accompanied by a structural transition from the O' phase to an almost

cubic—on the average undistorted—phase, known as the O^* phase (Fig. 1). A question that raises in this context is the role of the crystal structure in the nature of the paramagnetic (PM)-FM phase transition and the CMR effect. Detailed magnetization and transport properties measurements on both sides of the metal-insulator phase boundary, revealed the occurrence of a continuous second-order PM-FM phase transition in both the insulating and metallic regimes in LCMO and other relevant manganites.^{15,16} At first sight, this incurs the idea that the nature of the PM-FM phase transition is irrelevant to the underlying crystal lattice. However, a number of experiments^{17–19} have shown that close to optimal

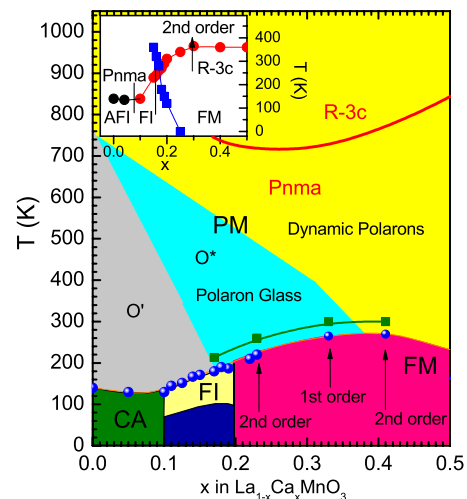


FIG. 1. (Color online) The phase diagram of $\text{La}_{1-x}\text{Ca}_x\text{MnO}_3$ for $0.0 \leq x \leq 0.5$. The polaron glass and dynamic polaron regimes are defined according to Ref. 23. The green squares (line) define the PM to FM transition line in magnetic field 9.4 T. The inset shows the corresponding phase diagram for $\text{La}_{1-x}\text{Sr}_x\text{MnO}_3$ from Ref. 31. The blue squares define the transition line between the $R\bar{3}c$ and Pnma crystal structures.

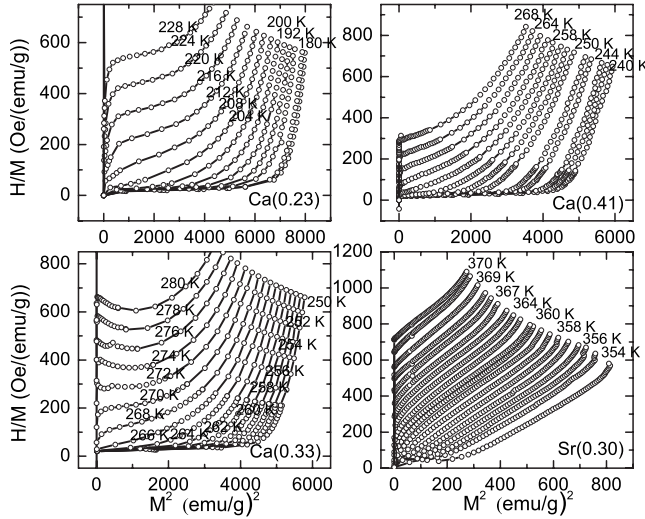


FIG. 2. H/M vs M^2 plots of isotherms in the vicinity of the Curie temperature T_c for LCMO(0.23,0.33,0.41) and LSMO(0.30) systems.

doping, $x \approx 0.33$, and in the region of T_c , nanoscale lattice polarons (local lattice and spin textures) are formed, which drive the PM to FM phase transition to first order.^{20–22} At the same time, neutron-scattering experiments, have shown that below a certain temperature T^* and in the temperature range $T_c \leq T \leq T^*$ polarons might form a glassy phase, which subsequently melts to a polaron fluid for $T > T^*$ (Refs. 23 and 24) (Fig. 1). Other experiments revealed that the anomalous first-order “like” phase transition is accompanied by frequency and temperature dependences,²⁵ and strong relaxation effects,^{26,27} which are reminiscent of relaxor ferroelectrics and spin glasses. Similar effects have been observed in $\text{Nd}_{0.70}\text{Sr}_{0.30}\text{MnO}_3$.²⁸ By contrast, no such effect have been observed in other optimally doped manganites (ODMs), such as $\text{La}_{0.70}\text{Sr}_{0.30}\text{MnO}_3$ [LSMO(0.30)], which exhibit a conventional second-order phase transition.^{20,22,29}

It is evident by now that the remarkable differences between ODM Ca-doped and Sr-doped systems are imposed by their different high-temperature crystal symmetry: In LCMO(0.33), a rhombohedral to orthorhombic ($R\bar{3}c$ to $Pnma$) phase transition occurs by cooling, at ≈ 700 K,³⁰ accompanied by the onset of strong collective JT distortions, while LSMO(0.33) remains in the rhombohedral $R\bar{3}c$ phase at all temperatures³¹ (inset of Fig. 1), where static JT displacements are forbidden by the crystal symmetry. However, it is unclear whether the observed “glassiness” in LCMO(0.33) is simply due to random freezing of polaronic distortions, or a collective spin-glass transition of the Ising type, driven by frustrated interactions and internal stresses.

Another puzzling issue is that by further increasing doping from $x=0.33$, where the stronger glassy phenomena are observed, the first-order PM-FM phase transition turns again to second order (Fig. 1). The subsequent transition from first to second order and then again to second order with increasing doping is clearly observed in Fig. 2, which demonstrates H/M vs M^2 isotherms of LCMO(0.23,0.33,0.41) and LSMO(0.30) in the vicinity of T_c . It is clearly seen that the

panel for $x=0.33$ shows negative slope in the lower M^2 region, which according to the Banerjee criterion^{20,32} is a clear sign that LCMO(0.33) belongs to the first-order transition. By moving away from optimal doping, in both directions, the slope becomes positive signifying that the transition becomes of the second order. However, in the lower doping regime, scaling arguments, which characterize second-order phase transitions are not directly applicable, and there are questions about the exact nature of the phase transition.²¹ In this context Salamon *et al.*³³ proposed that the CMR effect and the accompanying glassiness and slow relaxation effects in ODM manganites are consequence of a Griffiths phase, which is formed right above T_c , due to the presence of quenched disorder. However, recent magnetic-susceptibility measurements performed on LCMO(0.30) at low magnetic fields are against this scenario.³⁴

In order to shed more light to this difficult issue, we have performed ^{139}La and ^{55}Mn nuclear magnetic resonance (NMR) in the temperature range 80–900 K, on optimally doped LCMO(0.33) and LSMO(0.30) powder samples. For reasons of comparison, detailed ^{139}La NMR measurements as a function of temperature were performed on LCMO ($x=0.0, 0.11, 0.17, 0.23$, and 0.41) powder samples. In contrast to diffraction techniques, where long-range order with a coherence length of at least 100 nm is required, NMR is a local probe and therefore ideal for the characterization of short-range ordered systems. Our experiments suggest that in case of LCMO(0.33) strong local lattice distortions, apparently of polaronic origin,²³ are formed below the rhombohedral to orthorhombic transition temperature at ≈ 700 K. These distortions are responsible for the appearance of a spin-glass state in the PM phase, while for $T < T_c$ the spin-glass state merges with the FM phase, comprising a new thermodynamic phase (a kind of collective spin glass). The order in this novel phase resembles the order of spin glasses in a magnetic field, i.e., the long-range FM order and the short-range glassy order coexist. Contrary to reentrant spin-glass phases, by lowering temperature the growing FM order is shown to truncate the glassy phase component.

The experimental data are excellently simulated by using a simplified compressible random interaction-random field Ising Hamiltonian,³⁵ where strains induced by polaronic distortions are taken into consideration. In case of LCMO(0.33) a discontinuous change in the spin and Edwards-Anderson (EA) order parameters at T_c are foreseen by the model, while for $T < T_c$ the EA order parameter q_{EA} decays by decreasing temperature, in agreement with the experimental results. We notice that the EA order parameter q_{EA} in the FM state is defined by $\bar{q}_{EA} = q_{EA} - M^2$, where $q_{EA} = (1/N) \sum_i \langle S_i^2 \rangle = [\langle S_i^2 \rangle]_{av}$. The spin operator S_i takes the values ± 1 , $\langle \dots \rangle$ represents the time average, and $[\dots]_{av}$ denotes the disorder average. By moving away from optimal doping, lattice distortions faint out and the glassy component weakens rapidly, while the absence of an internal strain field is responsible for turning the phase transition from first order to second order.

II. MATERIALS AND METHODS

$\text{La}_{1-x}\text{D}_i\text{MnO}_3$ ($D_i = \text{Ca}$ and Sr) samples were prepared by thoroughly mixing high-purity stoichiometric amounts of

CaCO_3 (SrCO_3), La_2O_3 , and MnO_2 . The mixed powders formed in pastille form, reacted in air at 1400°C for several days with intermediate grinding and then slowly cooled down to room temperature. X-ray diffraction measurements were performed on a D500 SIEMENS diffractometer, showing that all samples are single phase materials with very good crystallinity. Magnetization measurements were performed on a Quantum Design MPMSR2 superconducting quantum interference device magnetometer. At temperatures higher than 350 K, magnetization measurements were performed on a Princeton Applied Research vibrating-sample magnetometer, model 155. The NMR experiments were performed on a home-built broadband spectrometer operating in the frequency range 5–800 MHz, in 9.4 T and zero external magnetic fields. Spectra were acquired by the spin-echo point by point method while varying the frequency because of the large spectral width of the resonance lines. An Oxford 1200CF continuous flow cryostat was employed for measurements in the temperature range 80–350 K and an Oxford HT1000V furnace for measurements in the range 300–900 K.

III. HIGH-TEMPERATURE ^{139}La NMR

The local magnetic and structural properties of the paramagnetic phase for all samples have been investigated by applying ^{139}La NMR in magnetic field 9.4 T, at temperatures as high as 900 K. In the presence of an external magnetic field B , $^{139}\text{La}(I=7/2)$ nuclei experience the Zeeman interaction, which splits the degenerate nuclear energy levels into $2I+1$ equidistant energy levels, with energies $E_m = m\gamma\hbar B$. In addition, the ^{139}La nucleus is coupled to the local electric field gradient (EFG) tensor, through its electric-quadrupole moment Q . We notice that a site with cubic symmetry has an EFG equal to zero; so the size of the effect of the electric-quadrupole interaction on the NMR spectrum measures the degree of deviation from cubic symmetry of the surroundings of the nuclear site. In the presence of the Zeeman and quadrupolar interactions the frequency of the NMR spectrum corresponding to transitions between levels m and $m-1$ is given by, $\omega_m = \gamma B + 3/2 e^2 q Q / 4\hbar I(2I-1)(3 \cos^2 \theta - 1 - \eta \sin^2 \theta \cos^2 \phi) (2m-1)$. Here, e is the charge of the electron, eq is equal to V_{zz} , η is the asymmetry parameter of the EFG tensor $0 \leq \eta = \frac{|V_{yy} - V_{xx}|}{V_{zz}} \leq 1$, and θ , ϕ are the angles between the principal axis of the EFG tensor and the magnetic field. In case of LCMO manganites, the magnetic field B at the site of the La nuclei is equal to the sum of the external field B and the transferred hyperfine field $B_{hf} = (1/\gamma\hbar)A\langle S \rangle$, where A is the hyperfine coupling constant and $\langle S \rangle$ the average electronic spin of the eight nearest Mn neighbors.^{36,37} In the PM phase, large frequency shifts proportional to the magnetic susceptibility are produced by the hyperfine coupling in the presence of an external magnetic field. According to the above equation, the transition between the $m=+1/2$ and $m=-1/2$ levels (the so-called central transition) is unaffected by the electric-quadrupole interaction to first order, while the distance in frequency of all other transitions (satellites) from the central transition, depends solely on the quadrupolar interaction. In a powder sample, the crystal axes, and hence the

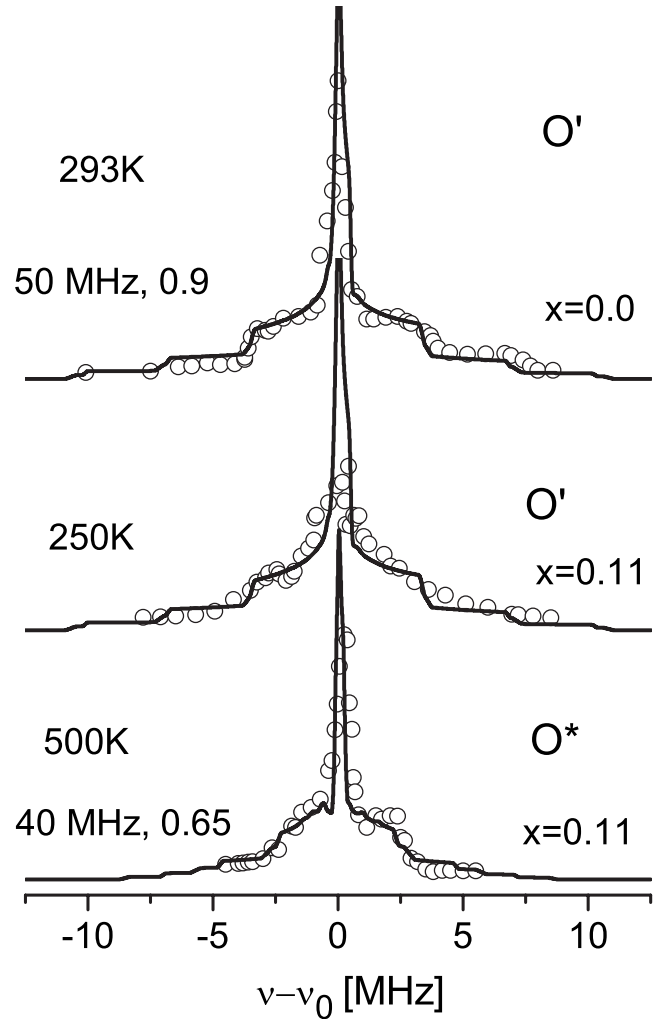


FIG. 3. ^{139}La NMR spectra for LCMO $x=0.0$ at 293 K and 0.11 at 250 and 500 K, in 9.4 T external magnetic field. Spectra are presented relatively to the central line frequency ν_0 . Open circles are experimental data and solid lines theoretical simulations.

EFG, are distributed at random angles with respect to the applied magnetic field. The angular average of the satellite patterns gives rise to a characteristic frequency distribution. The size of the satellite frequency distribution (SFD) is proportional to the EFG (and consequently to the lattice distortions) and independent of the magnetic field.

The ability of ^{139}La NMR, to provide information on the local crystal environment of LCMO systems becomes evident in Fig. 3, where spectra for $x=0.0$ at 293 K and $x=0.11$ at 250 and 500 K are demonstrated. Open circles are experimental data and solid lines theoretical simulations. In case of the pure system (O' phase at 293 K), an excellent agreement between the experimental data and the theoretical simulation is observed. For the simulation an electric quadrupolar coupling $\nu_Q = \frac{e^2 q Q}{h} = 50$ MHz, asymmetry parameter $\eta = 0.9$ and a dipole-dipole interaction of the La nuclear sites with the Mn ions of ≈ 20 kHz were considered, in agreement with previous works.^{38,39} The high ν_Q and η values are indicative of the strong coherent JT lattice distortion and charge and orbital anisotropy of the system. In case of x

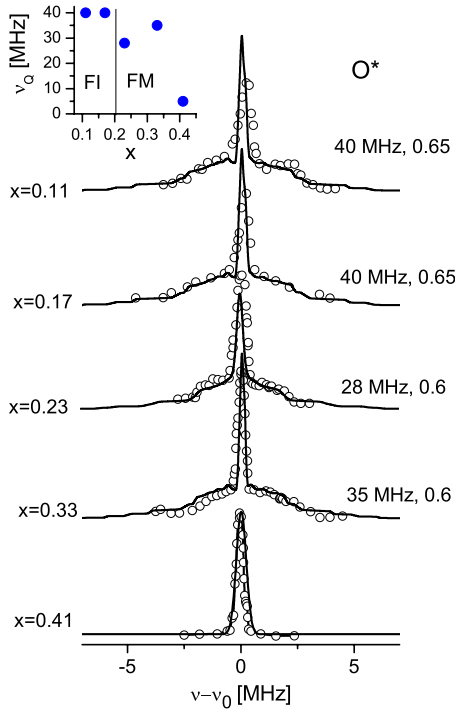


FIG. 4. (Color online) ^{139}La NMR spectra for LCMO $x=0.11, 0.17, 0.23, 0.33, 0.41$ at 500 K, in 9.4 T external magnetic field. Spectra are presented relatively to the central line frequency ν_0 . Open circles are experimental data and solid lines theoretical simulations. The inset indicates the electric quadrupolar coupling $\nu_Q = \frac{e^2qQ}{h}$ as a function of doping.

$=0.11$, at 250 K the system is also situated in the O' phase regime. By keeping the same simulation parameters as for $x=0.0$, it is observed that the SFD simulates quite well the experimental data, however the experimental central line is very broad, which indicates the presence of strong magnetic inhomogeneities. At 500 K the system is in the pseudocubic O^* phase, which explains the significant decrease in both the $\nu_Q=40$ MHz and $\eta=0.65$ values. The simulation of the central line fits also quite well with the experimental points, which is indicative of the absence of the strong magnetic inhomogeneities observed at lower temperatures.

Figure 4 demonstrates ^{139}La NMR spectra of the LCMO systems for $x= 0.11, 0.17, 0.23, 0.33, 0.41$ systems at 500 K. At this temperature all systems are in the O^* crystal phase. For $x=0.11$ and 0.17 spectra are almost the same, with $\nu_Q=40$ MHz and $\eta=0.65$. By further increasing doping the NMR powder pattern varies with doping significantly. For $x=0.23$ the ν_Q drops suddenly, increases at $x=0.33$, apparently due to the presence of strong polaronic distortions, and becomes vanishingly small for $x=0.41$. We notice the dramatic difference in the NMR SFD patterns between the $x=0.33$ and 0.41 samples, which according to Ref. 23 at high temperatures are both in the dynamic polaron regime. Contrary to this opinion, the NMR spectra in Fig. 4 indicate that the spin and lattice dynamics of the high-temperature phase of the two samples is completely different.

Figure 5 shows ^{139}La NMR spectra of LCMO(0.33) in the temperature range 320–900 K. At temperatures higher than 700 K spectra simulations give small $\nu_Q=21$ MHz and η

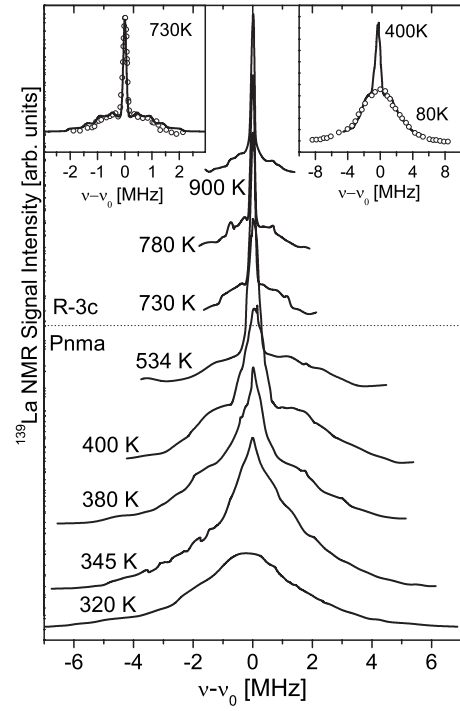


FIG. 5. ^{139}La NMR spectra for optimally doped LCMO(0.33), in 9.4 T external magnetic field, as a function of temperature. Spectra are presented relatively to the central line frequency ν_0 . The dotted line shows schematically the border line between the $R\bar{3}c$ and $Pnma$ phase regimes. The left inset depicts the calculated powder pattern spectrum in comparison to the experimental spectrum at $T=730$ K. The right inset shows a comparison of spectra at 80 K (open circles) and 400 K (solid line).

$=0.5$ values (inset in the top left side of Fig. 5). These small values are the fingerprint of the EFG in the $R\bar{3}c$ rhombohedral phase. By decreasing temperature, a significant increase in the SFD width is observed at $T \approx 700$ K, which marks the transition from the $R\bar{3}c$ to the $Pnma$ crystal structure,³⁰ and the appearance of strong incoherent JT displacements. For example, at $T=500$ K spectrum simulation values of $\nu_Q=35$ MHz and $\eta=0.6$ match excellently with the experimental spectrum, as shown previously in Fig. 4. This structural phase transformation is shown by synchrotron radiation measurements to be independent of the applied magnetic field.³⁰ Most remarkably, by further decreasing temperature, the average width of the SFD remains invariant down to the lowest measured temperature, as clearly seen in the inset at the top right side of Figs. 5 and 7. Hence, from the viewpoint of the La site, the size and distribution of local lattice distortions in the $Pnma$ phase does not appear to change by decreasing temperature. At the same time, the narrow central feature starts to broaden by cooling and disappears at ≈ 320 K, in agreement with previous measurements.⁴⁰ The extreme broadening of the central line, which up to first order depends solely to magnetic interactions, is a clear sign about the onset of a broad distribution of magnetic susceptibilities in the $Pnma$ phase on approaching T_c from above (the NMR signal broadening is proportional to the product of the magnetization and the susceptibility distribution width). Evi-

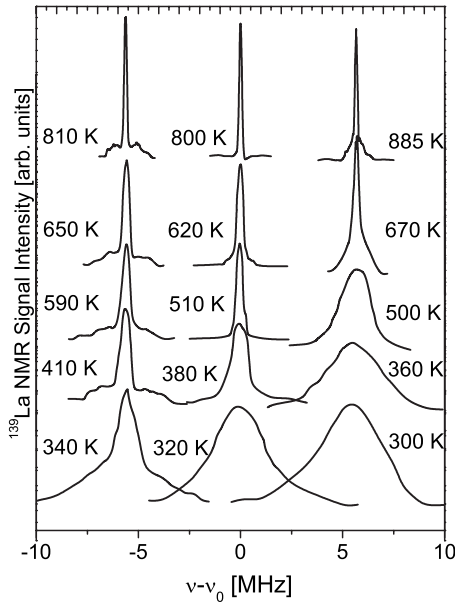


FIG. 6. ^{139}La NMR spectra for LCMO, $x=0.23$ (left), 0.41 (middle), and LSMO $x=0.3$ (right) at various temperatures. Spectra are presented relatively to the central line frequency ν_0 .

dently, the appearance of short-range correlated polarons,²³ produces a distribution of exchange couplings, which is directly reflected on the spin order of the system.

Figure 6 shows ^{139}La NMR spectra of the LCMO(0.23), LCMO(0.41), and LSMO(0.30) systems in the temperature range 300–885 K. In case of LCMO(0.23), at high-temperatures spectra depict the typical NMR powder pattern as in LCMO(0.33). However, two basic differences between the two systems are that (i) the SFD of LCMO(0.23) is at all measured temperatures sufficiently narrower than the SFD of LCMO(0.33), as clearly seen in the inset of Fig. 7 and (ii) the SFD width of LCMO(0.23) varies smoothly by decreasing

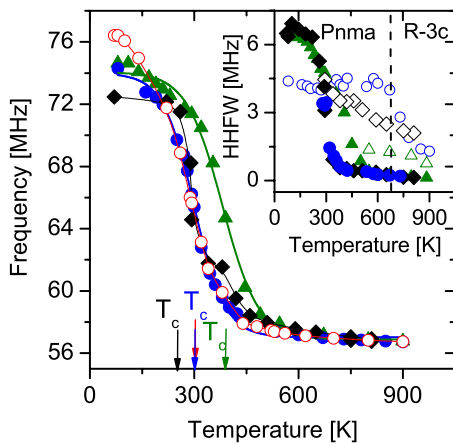


FIG. 7. (Color online) The ^{139}La NMR frequency as a function of temperature for LCMO(0.23) (\blacklozenge), LCMO(0.33) (\bullet), LCMO(0.41) (\circ), and LSMO(0.30) (\blacktriangle). In the inset the width of the NMR frequency distribution is shown for (i) LCMO(0.23) central line (\blacklozenge) and satellite powder pattern (\diamond), (ii) LCMO(0.33) central line (\bullet) and satellite powder pattern (\circ), and (iii) for LSMO(0.30) central line (\blacktriangle) and satellite powder pattern (\triangle).

temperature in the PM phase, while in LCMO(0.33), after increasing abruptly at $T \approx 700$ K, it remains invariant by lowering temperature (right inset in Fig. 5). At first sight this is a surprising result because LCMO(0.23) exhibits (i) transition from the $Pnma$ to the $R\bar{3}c$ phase at approximately the same temperature as LCMO(0.33) and (ii) neutron-scattering atomic-pair distribution function (PDF) analysis has shown that local JT distortions decrease by increasing Ca doping.⁴¹ A possible explanation is that close to doping $x=0.25$, small polarons might form an ordered lattice, where Mn^{4+} ions have six neighboring JT distorted Mn^{3+} sites, fitting together in a space filling three-dimensional network, which minimizes lattice distortions and strains.⁴² We notice that in case of LCMO(0.41) the SFD is almost absent and only the magnetic broadening of the central line is observed by decreasing temperature. This result is in agreement with the phase diagram in Fig. 1, which shows no static polarons for $x=0.41$ but rather the presence of dynamic polarons^{23,24} with a zero time average of local lattice distortions in the time scale of NMR experiments. Similar spectra but for different reasons are shown by LSMO(0.30). This system remains at all temperatures in the $R\bar{3}c$ rhombohedral phase (inset in Fig. 1), where static JT distortions are by symmetry forbidden, and therefore it depicts only a very narrow SFD while the central line broadens gradually by lowering temperature.

The above results are summarized in Fig. 7. The main panel shows the ^{139}La NMR frequency at 9.4 T as a function of temperature, for the four measured systems. The critical temperatures T_c , defined as the inflection point on the ν vs T curves, are found to be 260 K for LCMO(0.23), 300 K for LCMO(0.33) and LCMO(0.41) and 400 K for LSMO(0.30). These values (shown as green squares in Fig. 1) define the paramagnetic to ferromagnetic transition line at 9.4 T in the T - x phase diagram, which is parallel shifted to higher temperatures from the transition line in zero external magnetic field. We notice that although in second-order phase transitions critical temperature does not exist in the presence of a magnetic field, the observed temperature variation in the NMR frequency is fairly steep, indicating the existence of a phase transition or a crossover. Furthermore, it is observed that the transferred hyperfine field at saturation, expressed by the ^{139}La NMR frequency at 80 K, depends almost linearly on the doping concentration, in agreement with previous ^{139}La measurements in zero external magnetic field.³⁷

The uniqueness of ODM LCMO $x=0.33$, in comparison to lower and higher Ca doping, becomes obvious in the inset of Fig. 7, which shows the full width at half maximum of the central line for LCMO(0.23), LCMO(0.33), LCMO(0.41), and LSMO(0.30) (filled symbols), as well as the SFD for LCMO(0.23), LCMO(0.33), and LSMO(0.30) (open symbols). As previously discussed, in case of LCMO(0.33) the transition from the $R\bar{3}c$ to the $Pnma$ phase by cooling is clearly observed to occur at $T \approx 700$ K. Below that temperature, the abrupt increase in the SFD width declares the appearance of strong static local JT distortions, which remain invariant down to the lowest measured temperature. It is also clearly seen that the SFD width in the PM phase and thus the local lattice distortions, are in LCMO(0.33) by far the largest among the four measured systems. Another important notifi-

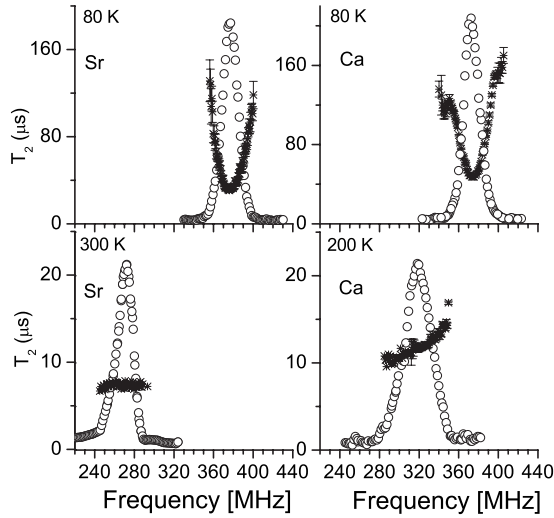


FIG. 8. ^{55}Mn NMR spectra in zero external magnetic field (open circles) of LCMO(0.33) at 80 K and 200 K and LSMO(0.30) (left figures) at 80 K and 300 K, respectively. The spin-spin T_2 relaxation times (crosses) as a function of frequency are also shown in the same figures. By increasing temperature spectra shift to lower frequencies while for LCMO(0.33) they become asymmetric broader on approaching T_c from below. The T_2 minimum at the peak of the spectra at 80 K is due to the Shul-Nakamura interactions.

cation is that contrary to LCMO(0.33) where the central line disappears at $T \approx 300$ K, apparently due to extreme inhomogeneous broadening, in the other three systems the central line remains visible at all temperatures, and its width varies with temperature in exactly the same way as the ^{139}La NMR frequency. This is a clear sign that—unlike to the LCMO(0.33) system—there is small distribution of magnetic susceptibilities.

IV. ^{55}Mn NMR MEASUREMENTS IN ZERO EXTERNAL MAGNETIC FIELD

The invisible with ^{139}La NMR “magnetic” glassy phase component for LCMO(0.33), is possible to monitor by applying ^{55}Mn NMR in zero external magnetic field. For reasons of comparison NMR data are compared with the prototype (in respect to the second-order nature of the phase transition) LSMO(0.30) system in the temperature range 80 K up to temperatures close to T_c .

^{55}Mn NMR in zero external magnetic field probes directly the electron-spin state of single Mn ions through the hyperfine field $B_{hf} = (1/\gamma\hbar)A(S)$, and therefore it is possible to resolve the different Mn charge states, i.e., localized Mn^{3+} , Mn^{4+} , and the intermediate FM valence states. Figure 8 shows ^{55}Mn NMR spectra for both samples at 80 K and 200 K (300 K), respectively. Spectra, as expected, were found to consist of a single line that is caused by motional narrowing, due to the fast electron hopping between the Mn^{3+} , Mn^{4+} manganese ions with frequency much higher than the NMR frequency.⁴³ In the same figure the nuclear spin-spin relaxation time T_2 as function of frequency is demonstrated. T_2 in manganites depends strongly on temperature,⁴⁴ apparently

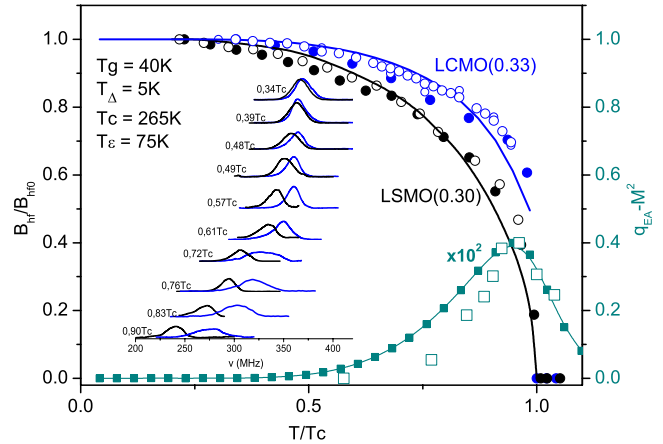


FIG. 9. (Color online) The hyperfine field B_{hf} as a function of temperature, obtained from ^{55}Mn NMR measurements, for LCMO(0.33) (blue, \circ) and LSMO(0.30) (black, \circ). The corresponding (blue and black, \bullet) are the B_{hf} values as obtained by Mössbauer spectroscopy on lightly Sn-doped samples from Ref. 22. The solid lines are theoretical fits by applying the self consistent Eqs. (5) and (6). Green filled squares (\blacksquare) present the EA order parameter, $\bar{q}_{EA} = q_{EA} - M^2$, as obtained by Eqs. (5) and (6). Green open squares (\square) correspond to the intensity of the quasielastic neutron-scattering component from Ref. 49. In conventional spin glasses, the quasielastic neutron-scattering component is considered to provide a measure of the EA order parameter. The inset shows the corresponding spectra for LCMO(0.33) (blue lines) and LSMO(0.30) (black lines).

due to fluctuations of the hyperfine field caused by hopping of the electron holes. At lower temperatures, an additional contribution to T_2 is observed, due to the Suhl-Nakamura relaxation mechanism,⁴⁵ which produces a characteristic T_2 minimum at the center of the spectra, in agreement with previous results.⁴⁶ This frequency dependence of T_2 disappears by increasing temperature. In case of LSMO(0.30) T_2 is shown to be frequency independent on approaching T_c from below. However, in LCMO(0.33) another frequency-dependent spin-dynamics appears, which is expressed as a monotonic increase in T_2 by increasing frequency. This effect indicates the presence of a distribution of low-frequency fluctuations close to T_c in LCMO(0.33), which is absent in LSMO(0.30).

At the same time, for $T > 150$ K a significant asymmetric broadening of the lineshape is observed in LCMO(0.33), which is absent in LSMO(0.30), in agreement with previous NMR works.^{43,46} This is clearly shown in Fig. 9, which demonstrates line shapes and the normalized hyperfine field $B_{hf}/B_{hf}(0)$ for both systems as a function of temperature. For reasons of comparison the $B_{hf}/B_{hf}(0)$ values obtained with Mössbauer spectroscopy from Ref. 22 are also presented in the same figure. An excellent match between the NMR and the Mössbauer hyperfine fields is observed. Another important experimental feature is that at T_c an abrupt decrease to zero of B_{hf} is observed for LCMO(0.33), which signals the first-order nature of the phase transition. On the contrary, in case of LSMO(0.30) the hyperfine field decreases continuously to zero by approaching T_c from below, as expected for a second-order phase transition.

V. COMPRESSIBLE RANDOM INTERACTIONS AND RANDOM FIELDS ISING MODEL

The discontinuous hyperfine field variation at T_c and the inhomogeneous ^{55}Mn NMR line-shape broadening for $T < T_c$ observed in LCMO(0.33), are nicely explained by considering a simple Ising Hamiltonian, where random interactions and random fields, together with a strain field ϵ_v induced by strong local lattice distortions are taken into consideration,^{35,47}

$$\mathcal{H} = -\frac{1}{2} \sum_{ij} \left[J_{ij}^0 + \sum_v J_{ij}^v \epsilon_v \right] S_i S_j - \sum_i f_i S_i + \frac{1}{2} N \sum_v \tilde{C}_v \epsilon_v^2. \quad (1)$$

Here, $\tilde{C}_v = v_0 C_v$, C_v is the appropriate irreducible elastic constant, v_0 the unit-cell volume, and N the number of unit cells in the crystal. The random interactions J_{ij}^0 and random fields f_i , produced by the lattice distortions caused by short-range correlated polarons, are assumed to be independently distributed according to Gaussian probability densities,

$$P(J_{ij}^{(0)}) = \frac{1}{\sqrt{2\pi J^2}} \exp[-(J_{ij}^{(0)} - J_0)^2/2J^2], \quad (2)$$

$$P(f_i) = \frac{1}{\sqrt{2\pi\Delta}} \exp[-f_i^2/2\Delta]. \quad (3)$$

Minimizing the above Hamiltonian with respect to the strains, and thus eliminating the strains an effective Hamiltonian is obtained,

$$\mathcal{H} = -\frac{1}{2} \sum_{ij} J_{ij}^0 S_i S_j - \sum_i f_i S_j - \frac{1}{8N} \sum_v \frac{1}{\tilde{C}_v} \left[\sum_{ij} J_{ij}^v S_i S_j \right]^2. \quad (4)$$

This is an extension of the Sherrington-Kirkpatrick model,⁴⁸ which in the weak-randomness limit predicts coexistence of spin-glass and FM order.^{35,47,48}

In the replica-symmetric mean-field approximation,⁴⁸ the reduced magnetization and the EA order parameters are calculated by the self-consistent equations,^{35,47}

$$M = \frac{1}{\sqrt{2\pi}} \int_{-\infty}^{+\infty} dz \exp(-z^2/2) \tanh \left[\left(q_{\text{EA}} \frac{T_g^2}{T^2} + \frac{T_\Delta^2}{T^2} \right)^{1/2} z + \frac{T_c}{T} M + \frac{T_\epsilon}{T} M^3 \right], \quad (5)$$

$$q_{\text{EA}} = \frac{1}{\sqrt{2\pi}} \int_{-\infty}^{+\infty} dz \exp(-z^2/2) \tanh^2 \left[\left(q_{\text{EA}} \frac{T_g^2}{T^2} + \frac{T_\Delta^2}{T^2} \right)^{1/2} z + \frac{T_c}{T} M + \frac{T_\epsilon}{T} M^3 \right], \quad (6)$$

where $T_g = \sqrt{NJ}/k_B$, $T_\Delta = \sqrt{\Delta}/k_B$, $T_c = NJ_0/k_B$, and $T_\epsilon = \frac{N^2}{2} (\sum_v J_v^2 / \tilde{C}_v) / k_B$.³⁵ According to this model, when the width of the distribution of the random interactions is larger than the effective mean value of the interaction constants a mag-

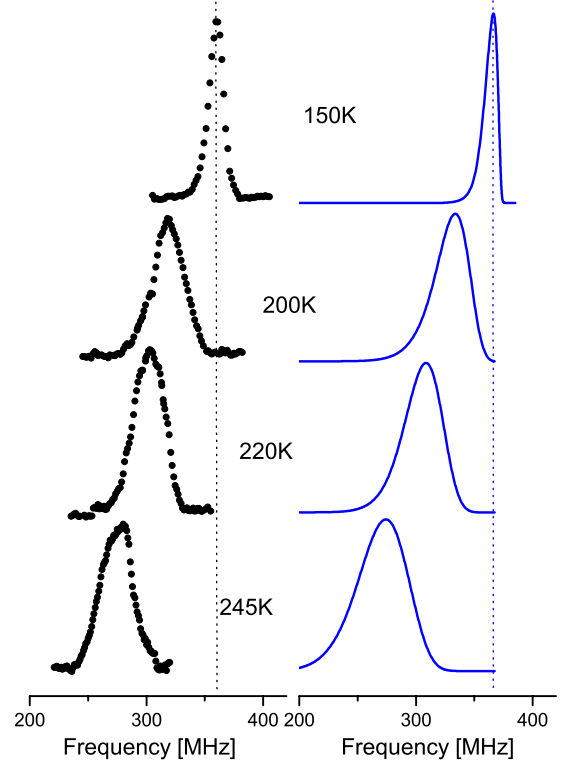


FIG. 10. (Color online) Experimental ^{55}Mn NMR line shapes (left) and theoretical simulations (right) for LCMO $x=0.33$ at various temperatures, as obtained by formula (7).

netic transition takes place, which drives the system from the PM to a pure spin-glassy state ($M=0, q_{\text{EA}} \neq 0$). In the opposite case, a PM to FM phase transition occurs, where the low-temperature FM phase coexists with a spin-glass state. We anticipate that this is the case in ODM LCMO(0.33).

By solving Eqs. (5) and (6) self-consistently, it is possible to fit the experimental $B_{hf}/B_{hf}(0)$ vs T curves in Fig. 9. In case of LCMO(0.33) data are fitted by considering $T_c = 265$ K, $T_g = 40$ K, $T_\Delta = 5$ K, and $T_\epsilon = 75$ K. This solution has a jump at T_c , in agreement with the experimental data. On the contrary, LSMO(0.30) is nicely fitted with a second-order phase transition, by ignoring both randomness and strain field. For $T > T_c$ Eq. (6) implies that $q_{\text{EA}} = \frac{T_\Delta^2}{T^2}$, i.e., the EA order parameter decays by increasing temperature. This is in agreement with the ^{139}La NMR results presented in Figs. 5 and 7, where the appearance and gradual narrowing of the central-transition NMR line at temperatures higher than 320 K, indicates the suppression of the spin-glass phase component at elevated temperatures. In a similar way, the effective EA order parameter \bar{q}_{EA} is shown to decay rapidly in the FM phase by decreasing temperature (Fig. 9). We notice the similarity of the temperature dependence of \bar{q}_{EA} with the intensity of the observed quasielastic neutron-scattering component,⁴⁹ close to T_c , [green open squares (\square) in Fig. 9], which in spin glasses is considered to provide a measure of the spin-glass order parameter. In case of ODM LCMO the appearance of the inelastic central component is attributed to the spin part of the correlated polaron glass with correlation length ≈ 1 nm.^{17,23}

On the basis of Eq. (6) it is possible to calculate the local magnetization function $W(m)$ (Ref. 35) and the NMR frequency distribution $f(\nu)$ [the latter is related to $W(m)$, by formula $f(\nu)d\nu=W(m)dm$],⁴⁷

$$f(\nu) \propto W(m) = \frac{1}{\left[2\pi\left(q_{EA}\frac{T_g^2}{T^2} + \frac{T_\Delta^2}{T^2}\right)\right]^{1/2}} \frac{1}{1-m^2} \times \exp\left\{-\frac{\left[\operatorname{arctanh}(m) - \frac{T_c}{T}M - \frac{T_\varepsilon}{T}M^3\right]^2}{2\left(q_{EA}\frac{T_g^2}{T^2} + \frac{T_\Delta^2}{T^2}\right)}\right\}. \quad (7)$$

By using the fitting parameters from Fig. 9 and Eq. (7) an excellent agreement is observed between the experimental and the simulated LCMO(0.33) line shapes, as shown in Fig. 10. Evidently, the observed ⁵⁵Mn NMR lineshape broadening in LCMO(0.33) by approaching T_c from below, is a sign of coexistence of long-range FM order and short-range spin-glass order, which accompanies the appearance of polaronic lattice distortions in this temperature region.

VI. CONCLUSIONS

On the basis of our experimental results we anticipate that optimally doped LCMO(0.33) shows a unique magnetic behavior in comparison to all other measured systems, by vary-

ing the temperature across T_c . Specifically, by entering the orthorhombic $Pnma$ crystal structure at $T \approx 700$ K on cooling, a broad distribution of strong lattice distortions appears, apparently of polaronic origin,²³ which in turn induces an equally broad inhomogeneous distribution of Mn electron-spin polarizations. Short-range correlations of such polaronic distortions^{23,24} appear to give rise to a spin-glass state, which for $T < T_c$ coexists with the FM order, but it gradually disappears by further decreasing temperature. This is in accordance with inelastic neutron-scattering experiments, which show the appearance of a strong quasielastic component with maximum intensity at T_c .^{17,49} We emphasize that this genuine “collective” spin-glass state is not produced by quenched disorder but is self generated and depends only on the competition among generic interactions such as magnetic exchange and JT interactions. Important role is played by the magnitude of lattice frustration, which creates an inhomogeneous strain field that controls the stability of the glassy state and the kind of the magnetic phase transition (first or second order). It is interesting to note that in the simplified model Ising Hamiltonian we have used, simulations show that the induced randomness on effective J couplings dominates in comparison to random fields created by trapped polaronic charge carriers. Indeed, changes in the J couplings (produced by local variations in the Mn-O bond lengths) are expected to have a sufficiently stronger effect than the weak random dipolar fields.

¹H. A. Mook and F. Dogan, *Nature (London)* **401**, 145 (1999).
²G. B. Teitelbaum, B. Büchner, and H. de Gronckel, *Phys. Rev. Lett.* **84**, 2949 (2000).
³J. M. Tranquada, D. J. Buttrey, V. Sachan, and J. E. Lorenzo, *Phys. Rev. Lett.* **73**, 1003 (1994).
⁴J. M. Tranquada, B. J. Sternlieb, D. Axe, Y. Nakamura, and S. Ushida, *Nature (London)* **375**, 561 (1995).
⁵E. Dagotto, T. Hotta, and A. Moreo, *Phys. Rep.* **344**, 1 (2001).
⁶M. Fäth, S. Freisem, A. A. Menovsky, Y. Tomioka, J. Aarts, and J. A. Mydosh, *Science* **285**, 1540 (1999).
⁷N. Mathur and P. Littlewood, *Phys. Today* **56**, 25 (2003).
⁸Y. Murakami, J. H. Yoo, D. Shindo, T. Atou, and M. Kikuchi, *Nature (London)* **423**, 965 (2003).
⁹N. D. Mathur, G. Burnell, S. Isaac, T. J. Jackson, B.-S. Teo, J. L. Macmanus-Driscoll, L. F. Cohen, J. E. Evetts, and M. G. Blamire, *Nature (London)* **387**, 266 (1997).
¹⁰J. Schmalian and P. G. Wolynes, *Phys. Rev. Lett.* **85**, 836 (2000).
¹¹C. Panagopoulos and V. Dobrosavljevic, *Phys. Rev. B* **72**, 014536 (2005).
¹²M. H. Julien, A. Campana, A. Rigamonti, P. Carretta, F. Borsa, P. Kuhns, A. P. Reyes, W. G. Moulton, M. Horvatic, C. Berthier, A. Vietkin, and A. Revcolevschi, *Phys. Rev. B* **63**, 144508 (2001).
¹³S. Chatterjee and A. K. Nigam, *Phys. Rev. B* **66**, 104403 (2002).
¹⁴G. Papavassiliou, M. Belesi, M. Fardis, and C. Dimitropoulos, *Phys. Rev. Lett.* **87**, 177204 (2001).
¹⁵W. Jiang, X. Z. Zhou, G. Williams, R. Privezentsev, and Y. Muk-

ovskii, *Phys. Rev. B* **79**, 214433 (2009).
¹⁶W. Jiang, X. Z. Zhou, G. Williams, Y. Mukovskii, and K. Glazyrin, *Phys. Rev. B* **78**, 144409 (2008).
¹⁷C. P. Adams, J. W. Lynn, Y. M. Mukovskii, A. A. Arsenov, and D. A. Shulyatev, *Phys. Rev. Lett.* **85**, 3954 (2000).
¹⁸P. Dai, J. A. Fernandez-Baca, N. Wakabayashi, E. W. Plummer, Y. Tomioka, and Y. Tokura, *Phys. Rev. Lett.* **85**, 2553 (2000).
¹⁹J. Zhang, P. Dai, J. A. Fernandez-Baca, E. W. Plummer, Y. Tomioka, and Y. Tokura, *Phys. Rev. Lett.* **86**, 3823 (2001).
²⁰J. Mira, J. Rivas, F. Rivadulla, C. Vazquez-Vazquez, and M. A. Lopez-Quintela, *Phys. Rev. B* **60**, 2998 (1999).
²¹F. Rivadulla, J. Rivas, and J. B. Goodenough, *Phys. Rev. B* **70**, 172410 (2004).
²²E. Assaridis, I. Panagiotopoulos, A. Moukarika, and T. Bakas, *Phys. Rev. B* **75**, 224412 (2007).
²³J. W. Lynn, D. N. Argyriou, Y. Ren, Y. Chen, Y. M. Mukovskii, and D. A. Shulyatev, *Phys. Rev. B* **76**, 014437 (2007).
²⁴D. N. Argyriou, J. W. Lynn, R. Osborn, B. Campbell, J. F. Mitchell, U. Ruett, H. N. Bordallo, A. Wildes, and C. D. Ling, *Phys. Rev. Lett.* **89**, 036401 (2002).
²⁵F. Cordero, C. Castellano, R. Cantelli, and M. Ferretti, *Phys. Rev. B* **65**, 012403 (2001).
²⁶R. H. Heffner, J. E. Sonier, D. E. MacLaughlin, G. J. Nieuwenhuys, G. Ehlers, F. Mezei, S.-W. Cheong, J. S. Gardner, and H. Röder, *Phys. Rev. Lett.* **85**, 3285 (2000).
²⁷R. D. Merithew, M. B. Weissman, F. M. Hess, P. Spradling, E. R. Nowak, J. O'Donnell, J. N. Eckstein, Y. Tokura, and Y. To-

- mioka, *Phys. Rev. Lett.* **84**, 3442 (2000).
- ²⁸J. A. Fernandez-Baca, P. Dai, H. Y. Hwang, C. Kloc, and S.-W. Cheong, *Phys. Rev. Lett.* **80**, 4012 (1998).
- ²⁹K. Ghosh, C. J. Lobb, R. L. Greene, S. G. Karabashev, D. A. Shulyatev, A. A. Arsenov, and Y. Mukovskii, *Phys. Rev. Lett.* **81**, 4740 (1998).
- ³⁰J. A. Souza, H. Terashita, E. Granado, R. F. Jardim, N. F. Oliveira, Jr., and R. Muccillo, *Phys. Rev. B* **78**, 054411 (2008).
- ³¹A. Asamitsu, Y. Moritomo, R. Kumai, Y. Tomioka, and Y. Tokura, *Phys. Rev. B* **54**, 1716 (1996).
- ³²S. K. Banerjee, *Phys. Lett.* **12**, 16 (1964).
- ³³M. B. Salamon, P. Lin, and S. H. Chun, *Phys. Lett.* **88**, 197203 (2002).
- ³⁴J. A. Souza, J. J. Neumeier, and Y. Yi-Kuo, *Phys. Rev. B* **78**, 014436 (2008).
- ³⁵G. Papantopoulos, G. Papavassiliou, F. Milia, V. H. Schmidt, J. E. Drumheller, N. J. Pinto, R. Blinc, and B. Zalar, *Phys. Rev. Lett.* **73**, 276 (1994).
- ³⁶G. Papavassiliou, M. Fardis, F. Milia, A. Simopoulos, G. Kallias, M. Pissas, D. Niarchos, N. Ioannidis, C. Dimitropoulos, and J. Dolinsek, *Phys. Rev. B* **55**, 15000 (1997).
- ³⁷G. Papavassiliou, M. Fardis, M. Belesi, M. Pissas, I. Panagiotopoulos, G. Kallias, D. Niarchos, C. Dimitropoulos, and J. Dolinsek, *Phys. Rev. B* **59**, 6390 (1999).
- ³⁸S. A. Lekomtsev, K. N. Mikhalev, A. Y. Yakubovskii, and A. R. Kaul, *J. Exp. Theor. Phys.* **102**, 671 (2006).
- ³⁹G. Allodi, M. C. Guidi, R. De Renzi, A. Caneiro, and L. Pinsard, *Phys. Rev. Lett.* **87**, 127206 (2001).
- ⁴⁰K. E. Sakaie, C. P. Slichter, P. Lin, M. Jaime, and M. B. Salamon, *Phys. Rev. B* **59**, 9382 (1999).
- ⁴¹E. S. Božin, M. Schmidt, A. J. DeConinck, G. Paglia, J. F. Mitchell, T. Chatterji, P. G. Radaelli, T. Proffen, and S. J. L. Billinge, *Phys. Rev. Lett.* **98**, 137203 (2007).
- ⁴²S. J. L. Billinge, T. Proffen, V. Petkov, J. L. Sarrao, and S. Kycia, *Phys. Rev. B* **62**, 1203 (2000).
- ⁴³G. Papavassiliou, M. Fardis, M. Belesi, T. G. Maris, G. Kallias, M. Pissas, D. Niarchos, C. Dimitropoulos, and J. Dolinsek, *Phys. Rev. Lett.* **84**, 761 (2000).
- ⁴⁴M. M. Savosta, V. A. Borodin, and P. Novak, *Phys. Rev. B* **59**, 8778 (1999).
- ⁴⁵J. H. Davis and C. W. Searle, *Phys. Rev. B* **9**, 323 (1974).
- ⁴⁶M. M. Savosta and P. Novak, *Phys. Rev. Lett.* **87**, 137204 (2001).
- ⁴⁷R. Blinc, J. Dolinsek, R. Pirc, B. Tadic, B. Zalar, R. Kind, and O. Liechti, *Phys. Rev. Lett.* **63**, 2248 (1989).
- ⁴⁸K. Binder and A. P. Young, *Rev. Mod. Phys.* **58**, 801 (1986).
- ⁴⁹J. W. Lynn, R. W. Erwin, J. A. Borchers, Q. Huang, A. Santoro, J.-L. Peng, and Z. Y. Li, *Phys. Rev. Lett.* **76**, 4046 (1996).